

1 **Bed erosion during fast ice streaming regulated the retreat**
2 **dynamics of the Irish Sea Ice Stream.**

3 **Katrien J. J. Van Landeghem¹ and Richard C. Chiverrell²**

4 ¹ *School of Ocean Sciences, Bangor University, Menai Bridge, LL59 5AB, UK*

5 ² *School of Environmental Sciences, University of Liverpool, Liverpool, L69 7ZT, UK*

6 **ABSTRACT**

7 Marine-terminating ice stream behaviour often defines the stability of ice sheets and is driven
8 by a complex interplay of climatic, oceanic, topographic and glaciological factors. Here, we
9 use new integrated high resolution, extensive (2100 km²) and continuous geophysical,
10 sedimentological and geotechnical data to reconstruct past glacial environments during the
11 Last Glacial Maximum from a well-preserved palaeo-landscape. The data is from the axial
12 centre of the Irish Sea Ice Stream (ISIS), which drained > 17% of the former British-Irish Ice
13 Sheet. Recent geochronological data of the palaeo-ISIS show a build-up and advance of ice to
14 marine-terminating maximum limits in the southern Celtic Sea 27–25 ka BP, followed by
15 rapid ice margin retreat into the northern Irish Sea Basin (ISB) by 20.8 ± 0.7 ka BP.
16 However, the flow dynamics in the central and axial bed of the ISIS through this timeframe
17 are not well understood. Here, we use our new glacial landscape reconstruction to identify the
18 spatial and temporal patterns of flow re-organisation and re-activations for the marine-
19 terminating ISIS. From this we infer how ice streaming was driven by a variety of factors
20 through advance, deglaciation and towards a temporary lift-off of ice from its bed and an
21 ultimate demise. Overprinted subglacial bedforms with differing ice flow directions indicate
22 an on/off behaviour to the ice-streaming, an increasing topographical influence and
23 substantial realignment of ice flows. Subsurface geophysical data reveal the erosive

24 capability of the ice stream through time, with a first erosive component in the formation of
25 mega-scale glacial lineations leaving bedrock exposed at the ice stream bed. The depositional
26 component of MSGL crest building occurred in the same ice-flow phase. Whilst the ice
27 stream was laterally constricted in two locations, likely contributing to changes in ice margin
28 retreat rates, we also propose that changes in basal drag associated with exposed bedrock at
29 the ice–bed interface influenced the retreat dynamics, particularly when this exposure was
30 near the grounding zone. The wider implications of this work are that episodic and highly
31 erosive ice streaming during ice advance and early retreat can change ice–bed conditions
32 radically and in turn influence glacial dynamics during later retreat episode, thus constituting
33 a feedback process to be considered in modelling the dynamics of marine-terminating ice
34 streams.

35 **KEYWORDS**

36 Quaternary; Glaciology (incl. palaeo-ice sheets); Europe; Geomorphology, glacial;
37 Geophysics; Subglacial Bedforms; British-Irish Ice Sheet; Palaeo-ice streaming; Deglaciation

38

39 **1. INTRODUCTION**

40 **1.1. Grounded ice stream dynamics and aim of the study**

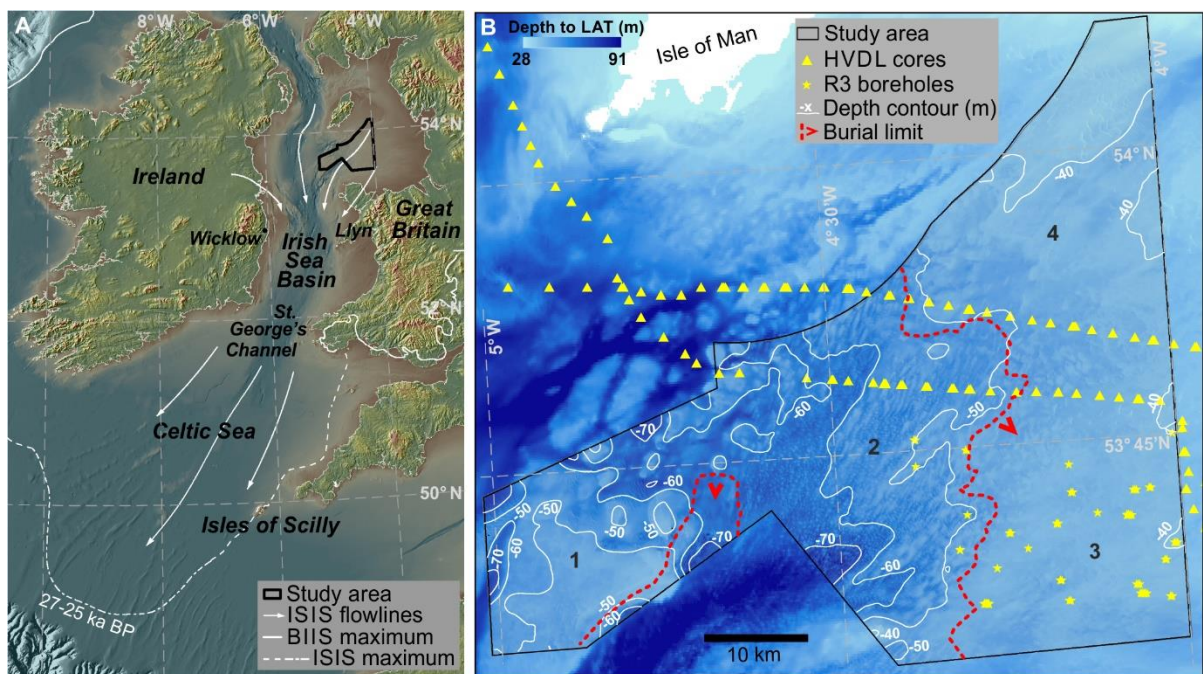
41 Deglaciation patterns of major ice sheets are determined by responses to climatic and
42 oceanographic changes (external forcing), topographic and basal thermal conditions (internal
43 forcing), with margin retreat rates varying by as much as an order of magnitude (Stroeven et
44 al., 2016). Ice streams are conduits of grounded ice flowing faster than adjacent areas
45 (Paterson, 1994) and account for most of the ice discharge in Antarctica (Bamber et al.,
46 2000). Realistic ice sheet drainage simulations therefore require knowledge of the onset of,
47 variations in, and shut-down of ice streaming (Jamieson et al., 2012; Schoof and Hewitt,

48 2016). The former Irish Sea Ice Stream (ISIS) drained >17% of the former British-Irish Ice
49 Sheet (BIIS). During the last deglaciation (25–18 ka BP) the ISIS experienced fluctuations
50 between rapid retreat (in the range 100–550 m a⁻¹), stabilisation and short-lived re-advances
51 of the ice margins (Chiverrell et al., 2018; Praeg et al., 2015; Scourse et al., 2019; Small et
52 al., 2018; Smedley et al., 2017a; Smedley et al., 2017b). Whilst the ice margin chronology of
53 ISIS is constrained well, no high-resolution shallow sub-seafloor information of the central
54 part of the ice flow conduit, the Irish Sea Basin (ISB – see Fig. 1) has thus far been integrated
55 to understand consecutive flow phases. We have only small snapshots of one preserved
56 surface of the former ice bed to inform us of the ice dynamical processes associated with the
57 ice margin fluctuations. On the seafloor NW of Anglesey, grounded ice streaming is
58 evidenced, and numerous iceberg scours show that retreat of the ISIS was in part
59 accompanied by a calving ice margin (Van Landeghem et al., 2009). New and extensive data
60 are provided here for both the surface and subsurface of the central sector of the ISB (see Fig.
61 1), making it an ideal testing ground for exploring subglacial evidence for changes in ice
62 stream dynamics during the well-dated advance, retreat and ultimate demise in the period of
63 27–18 ka BP.

64 Grounded marine margins can become unstable influencing ice sheet mass flux and rates of
65 deglaciation, with bed topography, subglacial bed properties and meltwater processes as first
66 order controls (Kleman and Applegate, 2014; Rignot et al., 2014; Bradwell et al., 2019). For
67 the former ISIS a high amplitude tidal regime and rising relative sea-levels (Bradley et al.,
68 2011; Ward et al., 2016) are further factors affecting potentially the stability of the ice
69 margin. Observations of ice streams in the palaeo-domain can provide a longer temporal
70 range and more extensive spatial perspective to that available typically in the observational
71 ice stream record. For example, Lakeman et al. (2018) used geophysical, stratigraphical and
72 chronological data in the western Canadian Arctic to reconstruct a 250 km retreat of a

73 marine-terminating ice stream in ~250 years during the Younger Dryas. Direct comparison of
74 bedforms observed developing at contemporary ice stream beds with equivalent bedforms
75 from palaeo-ice streams, provides basis for interpretation of deglacial processes (Van
76 Landeghem et al., 2009) and surge-stagnation-reactivation cycles (Kurjanski et al., 2019).
77 Observations of how ice–bed interfaces have evolved through time can be discerned from
78 information on (sub-)seabed geophysical surveys (see reviews in Stokes, 2018) and provide
79 potentially important constraint for simulations of glacial dynamics (Hindmarsh, 2018).
80

80



81

82 Figure 1. Panel (A) shows the Irish Sea Basin (ISB) with indicative Irish Sea Ice Stream
83 (ISIS) flow lines and the maximum extent of the British-Irish Ice Sheet and ISIS at ca. 27–25
84 ka BP (Chiverrell et al., 2013; Praeg et al., 2015). Panel (B) shows the study area divided in 4
85 zones: (Zone 1) a western till plateau, (Zone 2) subglacial bedforms, (Zone 3) buried
86 subglacial bedforms, and (Zone 4) an eastern till plateau. The extent of the geophysical and
87 sedimentological data collected in preparation of a Round 3 (R3) Windfarm development

88 project is displayed, as are the High Voltage Direct Link (HVDL) cable installation cores.

89 Depth to seafloor is relative to the Lowest Astronomical Tide (LAT).

90

91 The aim of this study is to use reconstructed ISIS dynamics as a case study to explain the

92 processes behind changes in ice stream advance, retreat and fluctuations in relation to

93 geological factors of the subglacial bed. We achieve this by reconstructing the temporal and

94 spatial evolution of a palaeo-glacial landscape for the axial central sector of the ice stream

95 (Fig. 1A), contextualised by the palaeo-ISIS geochronology during the Last Glacial

96 Maximum (27–18 ka BP – see next section). A new 2100 km² seabed geophysical and

97 sedimentological dataset is analysed to capture evidence of changing topography, sediment

98 distribution and glacial bedform assemblages from which we interpret changes in thermal

99 regime, bed topography, bed roughness, drainage patterns, ice flow direction and velocity for

100 the axial sector of the ISIS.

101 **1.2. The palaeo-ISIS geochronology**

102 The time series for grounded ice margin dynamics in this area is divided here into five stages.

103 The maximum extension of grounded ice reached the Celtic Sea shelf break around 27–25 ka

104 BP (Stage 1) (Praeg et al., 2015; Scourse et al., 2019; Smedley et al., 2017b). It then had

105 retreated rapidly by 400 km to the south coast of Ireland at 25.1 ± 1.2 ka BP (Stage 2),

106 eventually stabilizing at the constriction of the St-George's Channel at 24.2 ± 1.2 ka BP

107 (Small et al., 2018). The Irish Ice Sheet may have advanced into the Celtic Sea again (Tótz et

108 al., 2020), but the margin of the Irish Sea Ice Stream retreated rapidly towards the

109 constriction between Wicklow – Llŷn Peninsula at 22.6 ± 1 ka BP, where it stabilised (Stage

110 3) (Small et al., 2018; Smedley et al., 2017a). The western and deeper (100–140 m below

111 mean sea level (bmsl)) ISB had deglaciated by 19.8 ± 0.8 ka BP (Ballantyne and Ó Cofaigh,

112 2017; McCabe, 2008), whereas the retreat of ice margins in the adjacent shallower (50–20 m
113 bmsl) eastern ISB was slower crossing and moving north of the Isle of Man from 20.7 ± 0.7
114 and 19.3 ± 0.8 ka BP onwards (Stage 4) (Chiverrell et al., 2018). Stage 5 (between 19.3 ± 0.8
115 ka and 18.3 ± 1.1 ka BP) represents an ice-free study area, but a re-advance of Scottish ice on
116 the northern edge of the Isle of Man after 18.3 ± 1.1 ka BP may have seen ice encroach on the
117 area (Chiverrell et al., 2018).

118 **1.3. Glacial bedforms in palaeo-environmental reconstructions**

119 The type of glacial bedform can be indicative of cold- or warm-based basal conditions
120 (Kleman and Glasser, 2007; Kleman et al., 2006) whilst bedform geometry can reflect
121 changes in ice flow direction and relative changes in velocity (King et al., 2009; Landvik et
122 al., 2014; Stokes and Clark, 2002). Cold-based ice is below the pressure melting point with
123 no water available at the bed and has a limited ability to transport subglacial sediment and to
124 erode its bed. Thus cold-based ice is mainly associated with preservation of the pre-existing
125 land surface (Cuffey et al., 2000; Paterson, 1994). Warm-based ice is at the pressure melting
126 point with water available at the bed, and therefore associated with more intensive and
127 widespread erosion, deposition and reshaping of the subglacial bed (Kleman and Glasser,
128 2007; Paterson, 1994). Interpreting ice flow direction and velocity from subglacial bedforms
129 has contributed towards a better understanding of the basal thermal organisation and temporal
130 changes in flow regime for former ice streams (for example: Hogan et al., 2010).

131

132 **2. METHODS**

133 Our reconstruction of changing flow dynamics that characterised the collapsing ISIS stems
134 from new, extensive and high resolution geophysical and geotechnical evidence that
135 document a time and space continuum of an exceptionally preserved glacial landscape. The

136 evidence comprises the surface (multibeam data) and sub-surface (acoustic and geotechnical
137 data) expression of an assemblage of glacial bedforms. Acoustic, geotechnical and
138 sedimentological datasets were obtained for Celtic Array LTD for a proposed Round 3 (R3)
139 offshore wind development (Fig. 1B). From this integration of the geomorphological, sub-
140 bottom acoustic, sedimentological and sediment geotechnical evidence, we have mapped a
141 series of glacial bedform assemblages using ESRI ArcGIS software.

142 **2.1. Acoustic surveys**

143 The acoustic data were acquired by the Swedish surveying company MMT (Summer 2010).
144 Bathymetric data were collected with a ship-borne Kongsberg EM3002 Multibeam
145 Echosounder (MBES) and processed with CARIS HIPS by MMT. The EM3002 system uses
146 frequencies in the 300 kHz band, ideal for the shallow waters in this area of the Irish Sea (28–
147 92 m). The pulse length emitted by the EM3002 transducer is 150 μ s and the depth resolution
148 is 10 mm. Vessel positioning and orientation systems achieved a vertical accuracy < 5 cm
149 and a horizontal accuracy < 0.1 m. The bathymetric data were reduced to Lowest
150 Astronomical Tide (LAT), corrected with the UK Hydrographic Office Vertical Offshore
151 Reference Frame (VORF) model and gridded at 2×2 m. A total of circa 16500 km of sub-
152 bottom seismic data were collected using a 1kJ GeoSpark 200 tip Sparker source and a Chirp
153 Edgetech 512i (0.5–12 kHz) in a dense 2-dimensional grid at line spacings of 150 m and 500
154 m for cross-lines, all visualised with the KingdomSuite software package. This provided
155 shallow sub-bottom information with a vertical resolution up to 30 cm, from which bedrock
156 horizons and the top of over-consolidated tills were interpreted and digitised initially by
157 MMT. After a thorough review of the data analyses, the geophysical data outputs were
158 analysed further in ArcGIS. A multi-directional hillshading was applied to the bathymetric
159 grids, reducing a potential directional bias in bedform detection. Focal statistics were
160 performed on the irregular bathymetric surfaces to visualise the background break in slope,

161 whereby the mean bathymetric values were calculated in a raster with 500m cell size and
162 contour lines smoothed to eliminate the influence of the slope of smaller bedforms.

163 **2.2. Geotechnical and sedimentological surveys**

164 Seabed drilling was performed by Fugro Survey. The seabed drilling frame was positioned
165 using ultra-short baseline (USBL) acoustics with respect to Fugro's Starfix global positioning
166 system. Additional sediment descriptions were performed by Reynolds International Ltd. and
167 Parsons Brinckerhoff delivered a geotechnical interpretative report. These results were
168 integrated with other borehole surveys (Fig. 1B; 2) and the gridded seismic analyses to gain
169 confidence in the stratigraphic interpretations. Normally consolidated sand was generally
170 described as very loose to loose, slightly silty to silty gravelly fine to coarse sand, normally
171 consolidated clay as very soft to stiff slightly sandy slightly gravelly clay. Over-consolidated
172 sand was generally described as dense to very dense slightly silty to silty, gravelly fine to
173 medium sand. Band of gravels and cobbles and closely spaced thin laminae of clay have been
174 recorded in this unit. Over-consolidated clay was generally described as very stiff to very
175 hard slightly sandy to sandy, slightly gravelly clay. Soft bands occur within this unit.
176 Occasional soft bands and sand pockets are recorded within this unit, and a possible boulder.
177 Values for the key geotechnical parameters in Table 1, based on the Recommended Practice
178 for Statistical Representation of Soil Data (DNV, 2007), allowed normally consolidated and
179 over-consolidated sediments to be distinguished from soil profiles, and integrated with
180 seismic sub-bottom profiles. The thickness of the over-consolidated till (Fig. 4; 6; 8) was
181 derived from subtracting Two-Way-Travel Times (TWT) from sound waves reflecting off the
182 top of the bedrock with the TWT from sound waves reflecting off the top of the over-
183 consolidated till (Fig. 6). The speed of sound through the sediments is variable (for example
184 $1700\text{--}2700\text{ ms}^{-1}$ measured for clay) and conversion from TWT to meters can only be
185 estimated.

Parameter	Profile	Normally consolidated clay	Normally consolidated sand	Over-consolidated clay	Over-consolidated sand
Relative density (%)	characteristic lower bound		7		40
	characteristic mean		65		85
Undrained shear strength (kPa)	characteristic lower bound	10		50	
	characteristic mean	50		300	
CPT tip resistance (MPa)	characteristic lower bound	0.3	2	4	5
	characteristic mean	1.2	15	10	30

187 Table 1. Values for the key parameter for the normally and over-consolidated sediments,
188 measured and reported on by Parsons Brinckerhoff.

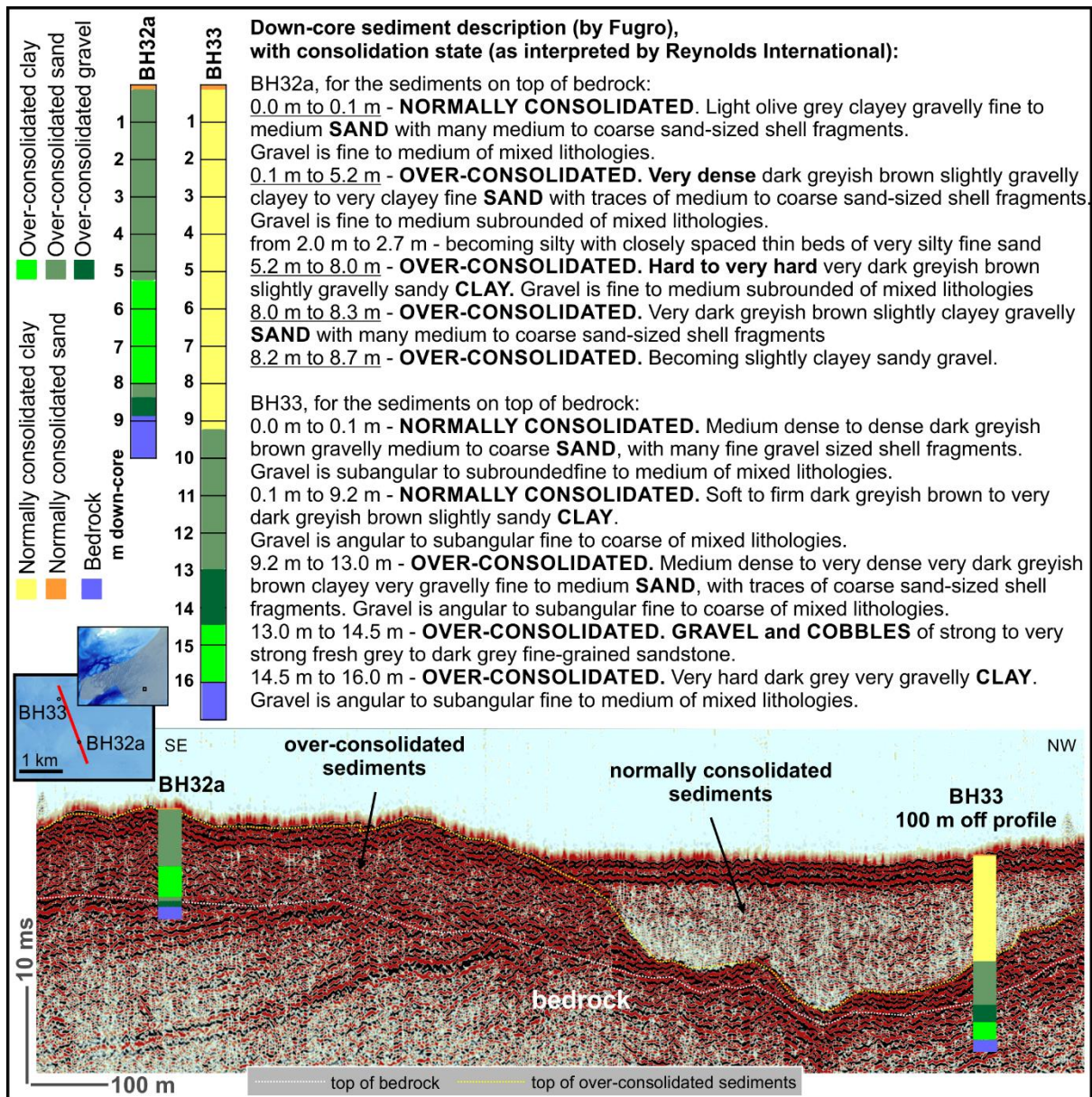
189

190 3. OBSERVATIONS AND INTERPRETATIONS

191 3.1 Stratigraphic units underpinning interpretation of the glacial landscape.

192 The stratigraphy of the sub-surface can be summarised as normally consolidated sediments,
193 over-consolidated sediments and bedrock, and these divisions underpin the interpretations of

194 the glacial landscape. Boreholes (BH) 32a and 33 are representative of this simplified
195 lithostratigraphy. They were recovered along a sub-bottom profile with lateral variation in
196 acoustic properties, and the integration of borehole descriptions and sub-bottom profile is
197 presented in Fig. 2, taking 1800 ms^{-1} as the speed of sound through the sediments to match
198 the down-core depth in meters to two-way travel time in milliseconds. BH32a was extracted
199 exactly on the sub-bottom profile line. The down-core transition between over-consolidated
200 sediments and the underlying mudstone corresponds with the high-amplitude seismic
201 reflector between chaotic acoustic facies with discontinuous internal reflections, and the
202 acoustic facies underneath with continuous internal reflections at a high angle and the upper
203 boundary reflection forming a sharp angular unconformity. BH33 is offset by 100 m from the
204 sub-bottom profile line, yet the transition between the normally consolidated sediments at the
205 top and the over-consolidated sediments underneath coincides with a clear distinction
206 between low-medium amplitude acoustic facies and high-amplitude acoustic facies
207 underneath. The transition to bedrock underneath is offset by circa three meters.
208



209

210 Figure 2. Integration of the sedimentological description of two boreholes with the sub-

211 bottom acoustic profile along which they were extracted.

212

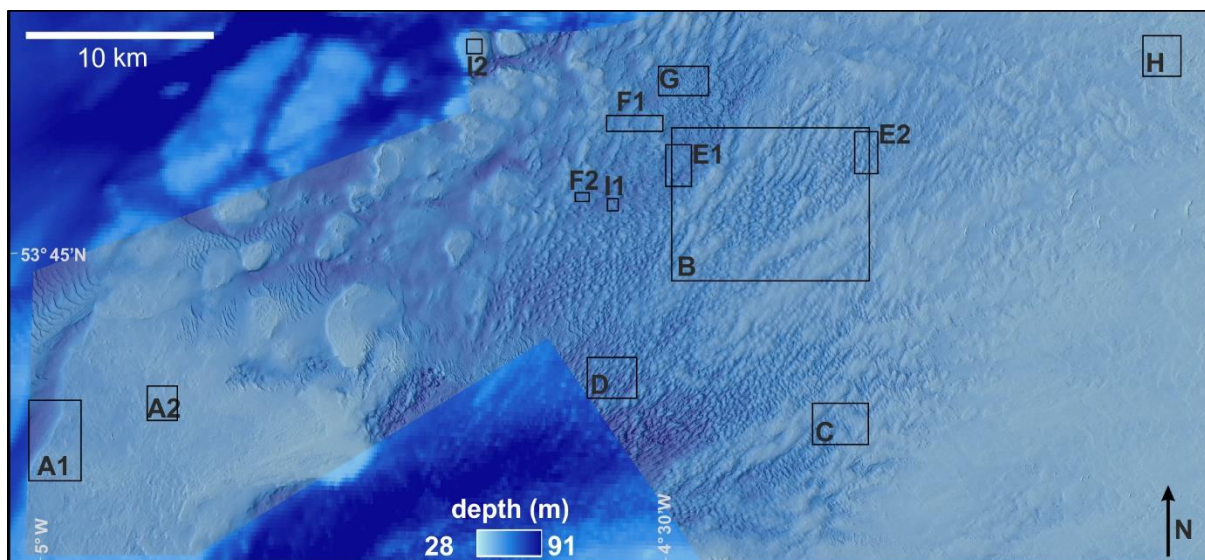
213 3.2 Mapping the glacial landscape with inferred ice flow directions

214 The bedform record in this study area is dominated by glacial bedforms. These bedforms


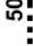






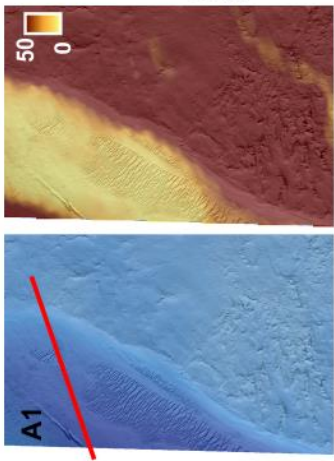
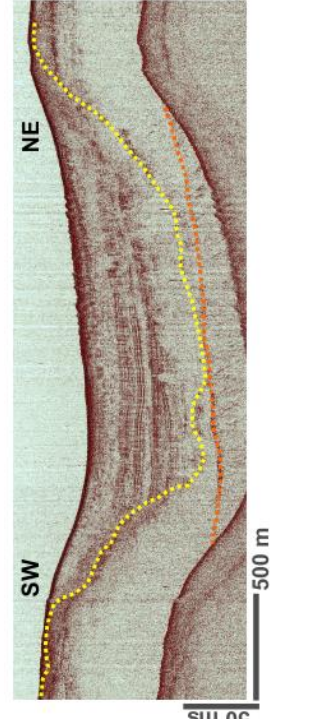

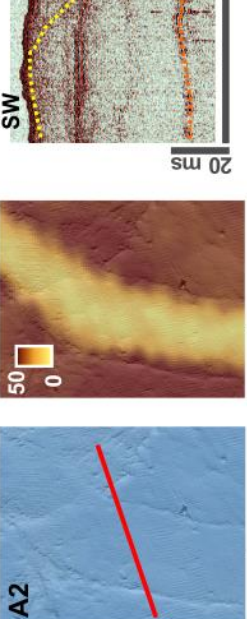
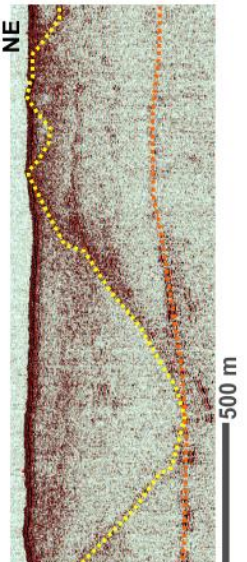

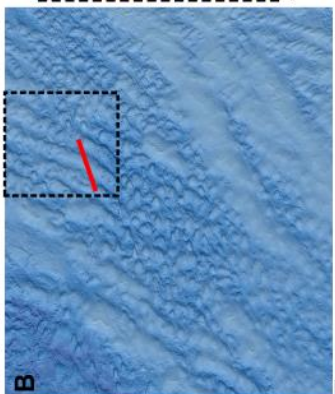
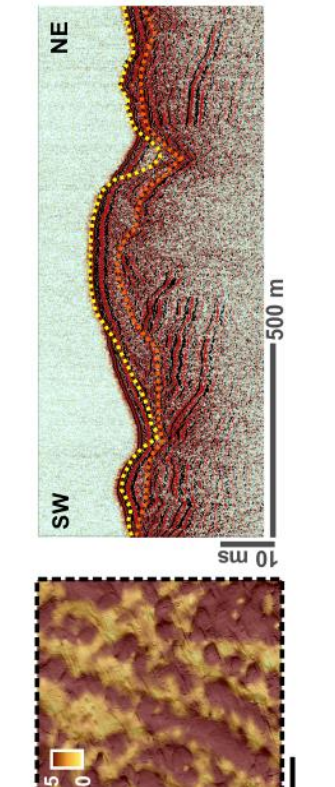

215 were mapped on both the seabed surface and in the sub-surface. With locations of examples

216 presented in Fig. 3., Fig. 4 summarises in three page-wide panels the interpretive lexicon used

217 for the glacial bedforms analysed in this area. From their geomorphological and spatial
218 analyses, it was possible to reconstruct the patterns of ice flow and to infer the changing
219 properties in subglacial bed conditions in the centre of the ISB. To assess wavelengths in
220 between flat topped subglacial bedforms, it was more accurate to delineate the trough in
221 between the bedforms, which had a steeper dip and could be better observed and delineated.
222 Groupings of glacial bedforms with typically a spatial extent $> 50 \text{ km}^2$ and a coherence in
223 terms of morphology, proximity and orientation are used here to identify a series of ice-flow
224 sets. To facilitate discussion of the bedform sequence, the glacial landscape is subdivided into
225 four broad morphological regions (Fig. 1B): (Zone 1) a western till plateau, (Zone 2)
226 subglacial bedforms, (Zone 3) buried subglacial bedforms, and (Zone 4) an eastern till
227 plateau.
228



230 Figure 3: Seabed bathymetry of study area illuminated with multi-directional hillshading,
231 identifying the location of exemplar bedforms presented in Fig. 4, where individual glacial
232 bedforms are shown and analysed.

<p>  Seabed bathymetry (m), thickness of over-consolidated till (TWT in ms), both with multi-directional hillshade of seabed bathymetry, and sub-bottom profile (SBP), located via </p> <p>    </p> <p>  </p> <th data-bbox="193 414 323 779"> <p>Description</p> <th data-bbox="193 190 323 414"> <p>Interpretation</p> <p><i>Ice flow</i> </p> </th></th>	<p>Description</p> <th data-bbox="193 190 323 414"> <p>Interpretation</p> <p><i>Ice flow</i> </p> </th>	<p>Interpretation</p> <p><i>Ice flow</i> </p>
 	<p>Channels cut through over-consolidated sediments, subsequently partly filled with normally consolidated sediments</p>	<p>Subglacial drainage channels. </p>
 	<p>Channels cut through over-consolidated sediments, subsequently entirely filled with normally consolidated sediments</p>	<p>Subglacial drainage channels. </p>
 	<p>Elongated bedforms from over-consolidated sediments, often partly eroded into bedrock. Thicker sediment deposits on bedform crest (consistent with ploughing process). Length >35 km, fragmented (overprinting by smaller subglacial bedforms). Elongation ratio >60:1, spacing 500–1000 m.</p>	<p>Mega-scale Glacial Lineations (MSGs) (formed subglacially in direction of ice flow) </p>

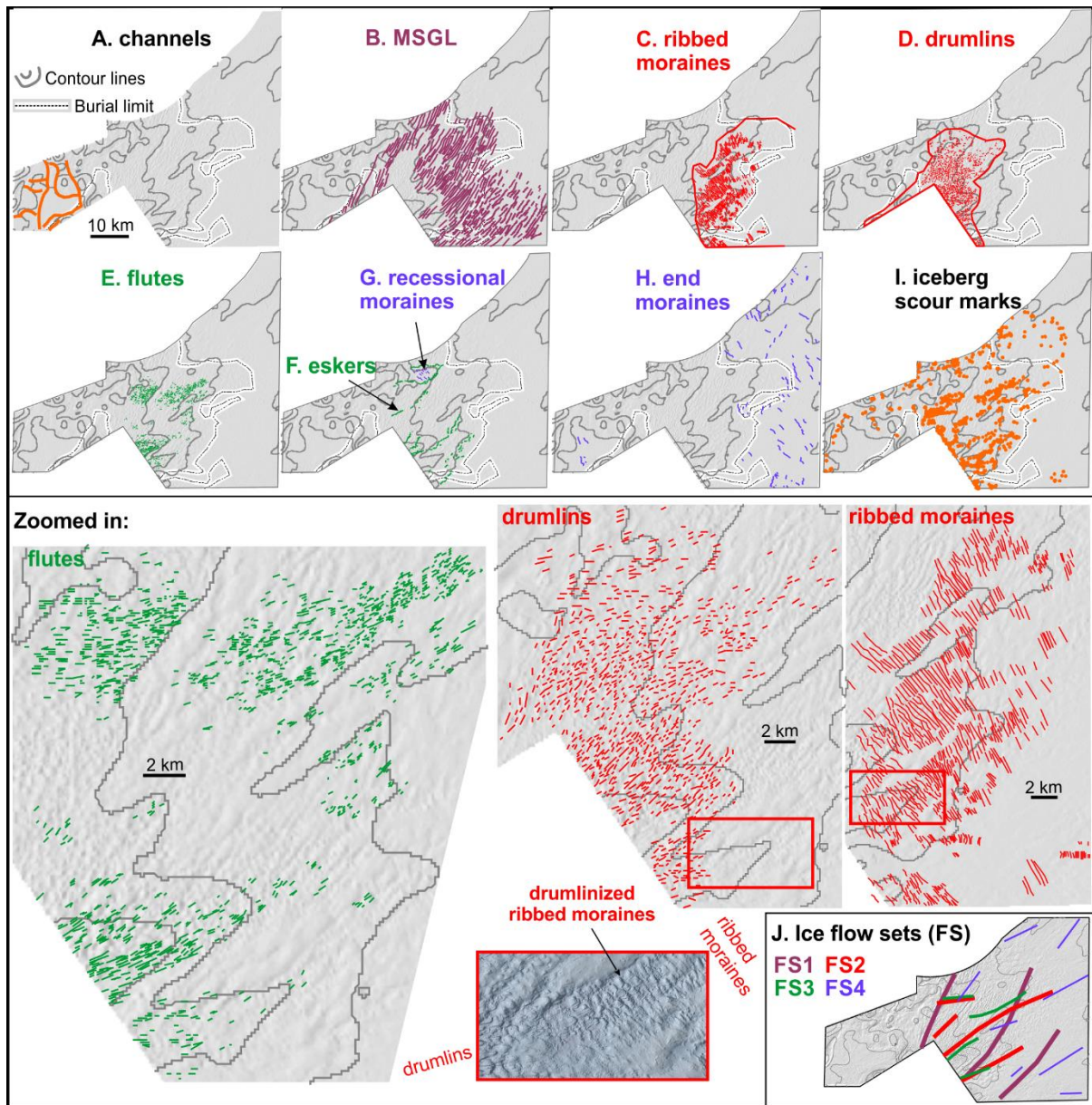
<p>Seabed bathymetry (m) with multidirectional hillshade and sub-bottom profile (SBP).</p> <p>depth (m) 28 91</p> <p>500m</p> <p>location SBP</p> <p>top of bedrock top of over-consolidated sediments</p>	<p>Description</p>	<p>Interpretation</p> <p>Ice flow</p>
<p>C</p> <p>SW NE</p> <p>part-buried bedform</p> <p>10 ms</p> <p>100 m</p>	<p>Elongated bedforms from over-consolidated sediments, typically 300–1000 m long, 100 m wide and 5–10 m high. Often fit neatly together like a jigsaw. Gentle slopes (rarely >10°) and variable symmetry. Smaller bedforms towards the SE. Bedforms found buried up to 20 m deep.</p>	<p>Ribbed moraines (formed subglacially transverse to direction of ice flow).</p>
<p>D</p> <p>SW NE</p> <p>part-buried bedform</p> <p>buried tail of adjacent bedform</p> <p>10 ms</p> <p>100 m</p>	<p>Elongated bedforms from over-consolidated sediments, sometimes partly eroded into bedrock. Tapered side towards deeper ISB. Elongation ratios < 15:1. Length typically 500 m, width 150–250 m, height 10–15 m. Steep eastern slopes (< 30°).</p>	<p>Drumlins (formed subglacially in direction of ice flow).</p>
<p>E1</p> <p>E2</p> <p>flutes</p> <p>flute overprinting drumlin</p> <p>SE NW</p> <p>10 ms</p> <p>100 m</p> <p>derived from neighbouring lines and cross lines</p>	<p>Small bedforms from over-consolidated sediments, partly overprinting drumlins (left) and ribbed moraines (right). They are typically 100–150 m long, 20–50 m wide and 1–2 m high. Too small to detect in the subsurface.</p>	<p>Flutes / flutings (formed subglacially in direction of ice flow).</p>

<p>Seabed bathymetry (m) with multidirectional hillshade and sub-bottom profile (SBP).</p> <p> </p>	<p>Description</p>	<p>Interpretation</p> <p><i>Ice flow</i> ↘</p>
<p>F1</p> <p>F2</p> <p>NE</p> <p>derived from neighbouring lines and cross lines</p>	<p>Long, winding ridge, up to 4 m high. Overprinting flutes, but some parts of the eskers have been streamlined as well.</p>	<p>Eskers (formed subglacially).</p>
<p>G</p> <p>NE</p>	<p>Ridges of diamiction, typically 5 m high, 1km (yet variable) in length, 100-150m wide, variable in asymmetry. Surficial sand ripples over the top of the features alter their shape in places.</p>	<p>Push moraines (formed near/at ice margin).</p>
<p>H</p> <p>NE</p>	<p>Ridges of diamiction, typically 2-3 m high. Fragmented, several kilometres long. Slightly steeper towards the eastern side.</p>	<p>End moraines (formed at ice margin).</p>
<p>I1</p> <p>I2</p> <p>NW</p>	<p>Parallel sets of berms around pit or elongated depression with various shapes & sizes. Round pits can be 100 m in diameter, 3 m deep. Small marks overprinting drumlins (left); long marks on a plateau of over-consolidated sediments (right).</p>	<p>Iceberg scour marks.</p>

236 Figure 4. Three panels with examples (A–I) of bedforms identified in the multibeam
237 echosounder data and sub-bottom profiles (SBP), with delineation of bedrock and over-
238 consolidated till surfaces on the acoustic profiles, description and interpretation of the
239 bedforms and the implied direction of ice flow.

240

241 Figure 5 presents maps of the axes of these individual bedforms identified and exemplified in
242 Fig. 4. Only the axes of the MSGL could be traced into the subsurface from the 500×150 m
243 grid of sub-bottom profiles. The precise axis of individual smaller and (partly) buried
244 bedforms could not be fully delineated from sub-bottom profiles, but their presence could be
245 detected. The ice-flow sets (FS) interpreted from these bedform assemblages are summarised
246 in Fig. 5J and in Fig. 8 and contextualised with the five stages of the advance and retreat
247 chronology for the ISIS defined in Section 1.2.



248

249 Figure 5. A–I: The axes of the individual bedforms as identified and exemplified in the panels
 250 of Fig. 4. Only the axes of the MSGL could be digitised from the sub-bottom profiles, so the
 251 axes of the ribbed moraines and drumlins only represent the bedforms present on the seabed
 252 surface. The areas with all ribbed moraines, drumlins and flutes have been zoomed in to
 253 better discern the direction of the longest axes of the bedforms, and a hillshaded seabed
 254 bathymetry displays the drumlinised ribbed moraines. J: schematic representation of ice-flow
 255 sets (FS) interpreted from these bedform assemblages and their overprinting relationships
 256 (Fig. 4).

257

258 **3.3 Mega-scale glacial lineations (MSGSLs) forming and exposing bedrock – ISIS**

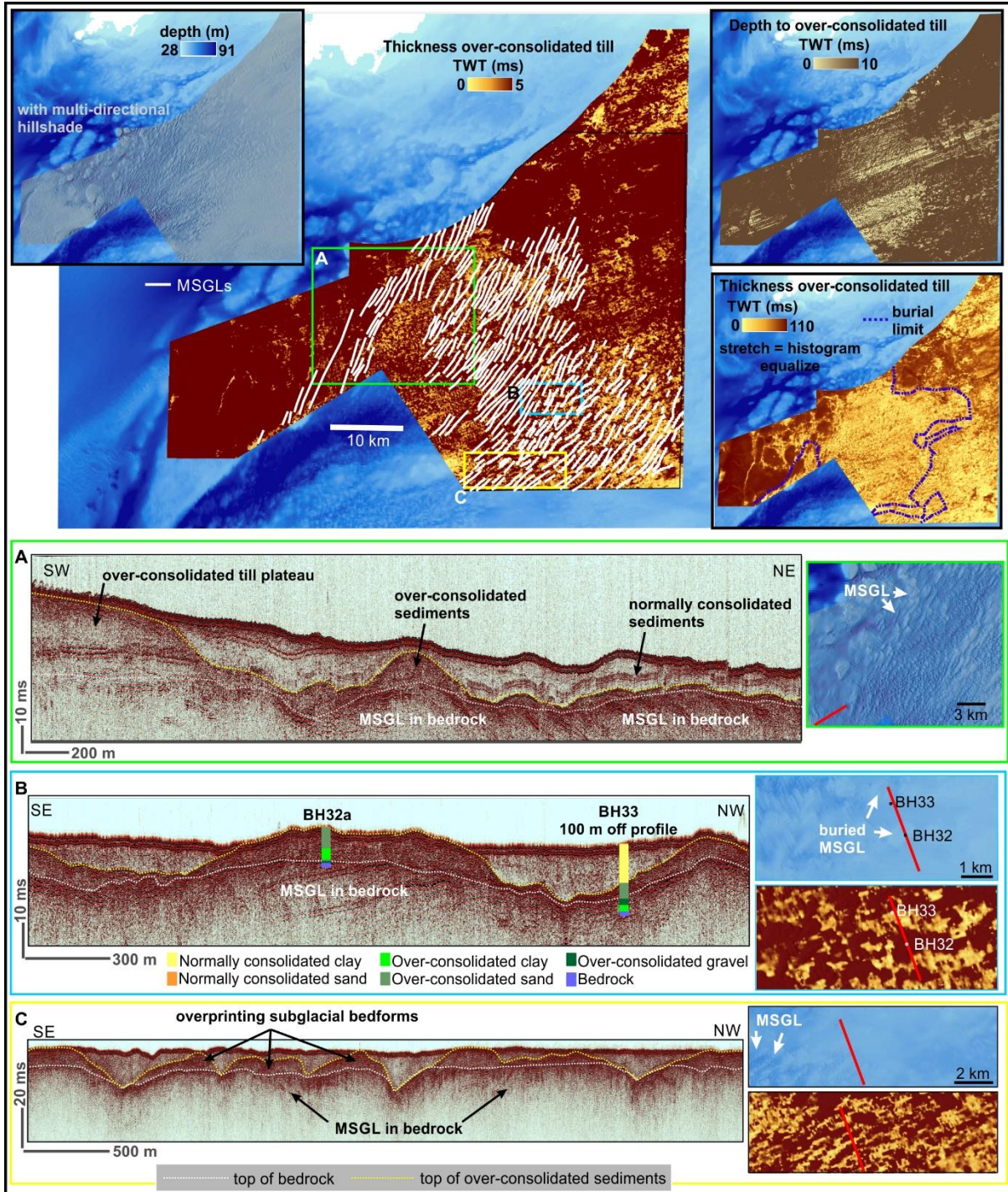
259 **maximum extent and rapid initial retreat**

260 The western till plateau (Zone 1) comprises over-consolidated tills that are incised by linear
261 channels (Fig. 4A) dissecting in places the entire sedimentary sequence with a similar NNE-
262 SSW orientation to the subglacial drainage systems on Anglesey (Lee et al., 2015). The
263 channels have been filled partially or fully by normally consolidated sediments, and some
264 infills post-date moraine formation on the plateau, as the crests of some moraines are
265 interrupted across the infilled channels (Fig. 4A). Thick accretionary wedges of normally
266 consolidated glacial sediments formed in places at the edge of the till plateau, seemingly
267 fed in part from these incised channels. This plateau of till has been eroded and the eroded
268 sediments moulded into a series of subglacial bedforms (Fig. 6), creating the central glacial
269 terrain with subglacial bedforms on the seabed surface (Zone 2).

270 Forming Flow Set (FS) 1, large-scale ridges of >30 km long, about 20–25 m high and with
271 elongation ratios approaching 60:1 occur as a broad 45 km wide swathe across this Zone 2.
272 Interpreted as mega-scale glacial lineations (MSGSLs – Fig. 4B; Fig. 6), these bedforms are
273 partly buried by normally consolidated sediments in the east of Zone 2 and their sizes
274 compare well with reported MSGSL (Spagnolo et al., 2014). The integration of BH 32a and
275 BH33 with the sub-bottom profile over an MSGSL exemplifies the differences in sediment
276 properties between the MSGSL crest and trough (Fig. 2; 6), with over-consolidated gravelly
277 sands and clays forming the MSGSL crest, and mainly normally consolidated gravelly clays
278 filling in the troughs between MSGSLs. Across the large study area the orientation of MSGSLs
279 gradually changes. In the northwest and central region of Zone 2, the MSGSLs are orientated
280 205°, parallel to the main axis of the ISB, but curve westerly 240° moving progressively

281 southeast (Fig. 5B;6), and thus guided probably by the topography of the island of Anglesey
 282 (Phillips et al., 2010 - Fig. 1).

283



284

285 Figure 6. Data of the surface and sub-surface expression of mega-scale glacial lineations
 286 (MSGLs) from 3D grids of depth to the seabed surface, depth to the over-consolidated till and

287 the thickness of the over-consolidated till. The latter was presented with both a linear color
288 gradient and with a stretched classification system using histogram equalisation to enhance
289 contrast across this large study area with large variations in till thickness. Panels A, B and C
290 display 2D seismic profiles perpendicular to the long axis of MSGSLs, with a depth scale in
291 Two-Way-Travel Time (TWT). Panel A shows the erosional edge of the subglacial till
292 plateau and subglacial bedforms buried underneath normally consolidated sediments and
293 formed partly erosional into the underlying bedrock. Panels B and C display partly and fully
294 buried subglacial MSGSLs constructed from erosion into bedrock and deposition of till.

295

296 A key interpretation integrated from the analysis of 16500 km of sub-bottom profiles, is that
297 the swathe of MSGSLs is flanked to the west, north and east by the remaining plateau of over-
298 consolidated till and that the MSGSLs have interspaced grooves that incise into the bedrock
299 (Fig. 6), creating lower-amplitude MSGSL in the bedrock surface over which over-
300 consolidated till was deposited (Fig. 2; 6). No meltwater-related deposits were observed on-
301 lapping the over-consolidated sediments in the MSGSLs and the bedrock in between the
302 MSGSLs is overlain by a very thin layer of over-consolidated till, or directly by normally
303 consolidated sediments. There is thus no evidence for bedforms to have formed via subglacial
304 floods, and the MSGSLs were seemingly formed via subglacial erosion into bedrock and
305 deposition of till. The bedrock, predominantly Carboniferous sand stones, siltstones and
306 mudstones in this area, was thus eroded into and left temporarily exposed as part of the
307 subglacial bed due to MSGSL formation. This erosional phase of ice streaming has an ISIS
308 axis-parallel alignment. To sustain ice flow parallel to the axis of the ISIS on the seafloor and
309 across Anglesey (Phillips et al., 2010) requires an ice front significantly to the south of the
310 constriction between Wicklow and the Llŷn Peninsula. This erosional phase is therefore
311 associated with geochronological Stages 1 and 2, during extension to maximum limits and/or

312 with ice streaming during the initial rapid retreat (27–25 ka BP) (Praeg et al., 2015; Scourse
313 et al., 2019; Smedley et al., 2017b, Small et al., 2018).

314 **3.4 Frozen bed and onset of warm-based ice streaming**

315 Fields of moraines (Fig. 4C) in the central Irish Sea Basin with often jigsaw-puzzle
316 arrangements have been interpreted as ribbed moraines (Van Landeghem et al., 2009), with a
317 formation mechanism of brittle fracture of frozen till aligned with that proposed by Kleman
318 and Hättestrand (1999). These ribbed moraines gradually evolve down-ice where moraines
319 start having a clearly tapered side interpreted as drumlins (Fig. 4D; Van Landeghem et al.,
320 2009), and can be explained by time and space transgressive model by Kleman and
321 Hättestrand (1999) where this transition occurs due to a phase change of frozen bed to thawed
322 bed. The data presented here, show that ribbed moraines and drumlins overprint the MSGL
323 terrain (Fig. 3; 5B–D). The ribbed moraines are transversely orientated to a 225–255 °N ice
324 flow and display evidence for topographical focusing of ice flow as the long axes of ribbed
325 moraines are transverse to ice flow direction, and these axes broadly follow the contour lines
326 of the background bathymetry (Fig. 5C). Identical ice flow alignment is displayed by the
327 drumlins, elongated parallel to the ice flow direction, and together with the ribbed moraines
328 they form FS2. The area of drumlinised ribbed moraines between the ribbed moraine and
329 drumlin field (Fig. 5; Van Landeghem et al., 2009) reflects time-transgressive changes to a
330 lubricated and less rigid bed rheology (cf. Kleman and Hättestrand, 1999). Towards the
331 western steeper slopes of Zone 2, drumlin elongation ratios increase from <1.5:1 to 5:1 and
332 the converging directions of the long drumlin axes are indicative of a convergence of south-
333 westerly ice flows guided by the topography. To the east and south-east of Zone 2 the glacial
334 landscape is buried (Zone 3), and MSGLs, ribbed moraines and drumlins are visible in the
335 sub-bottom acoustic data (Fig. 4C; 4D). Both drumlins and ribbed moraines display an ice-
336 flow alignment more in keeping with geochronological Stage 3. This westerly - south-

337 westerly ice flow alignment corresponds with short-lived stabilisations of the ice margin at
338 the constriction of the Irish Sea between Wicklow and Llŷn Peninsula at 22.6 ± 1 ka BP
339 (Small et al., 2018; Smedley et al., 2017a), draw-down of the ice surface, greater
340 topographical focusing and the inception of ice-free marine conditions in the western ISB
341 (Chiverrell et al., 2018).

342 **3.5. Ice flows into ice-free western ISB**

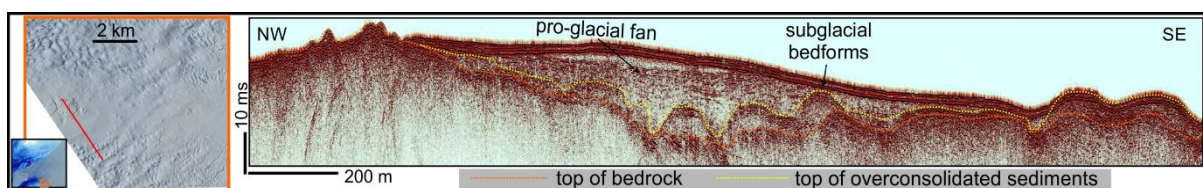
343 Smaller bedforms overprint and have moulded locally all the previous ice-flow sets and are
344 interpreted as flutes or flutings (Fig. 4E). The numerous lineations vary from a westerly
345 direction on flat seabed to a south-westerly direction where they are conditioned by and
346 follow the seabed topography (FS3 - Fig. 5E). The flutings often overprint multiple bedforms
347 (e.g. drumlins and ribbed moraines) and their dimensions of ~60 m wide and 1500 m long
348 approach those of mega-flutes (Bluemle et al., 1993). Formation of such elongated flutings
349 are primarily associated with a temperate and grounded glacial land-system (Evans and
350 Twigg, 2002; Stokes and Clark, 2002) and have been linked with surge type ice flow
351 behaviour and high basal ice velocities (Bluemle et al., 1993; Waller et al., 2008).

352 Our interpretation of flow sets 2 and 3 (ribbed moraines, drumlins and flutes), is that a phase
353 of reduced ice streaming allowed frozen bed conditions and ribbed moraines to form. A
354 resumption of warm-based ice streaming caused the drumlinisation of the ribbed moraines as
355 the thawing front moved eastwards. The subsequent ice flow surge stopped the thawing front
356 migrating eastwards and resulted in flutings over the top of drumlins and the most westerly
357 ribbed moraines. The ice margin then lifted off temporarily to preserve the remaining ribbed
358 moraines from further subglacial reworking.

359 Eskers are also preserved well in Zone 2 and their direction is seemingly controlled by the
360 changes in topography (Fig. 4F; 5F). Their spacing varies between 2 and 8 km and their

361 general direction aligns with the ice flow directions derived from FS2 (ribbed moraines and
362 drumlins). They are found mostly superimposed on FS1–3 (MSGLs, ribbed moraines,
363 drumlins and flutes) (Fig. 5F), but occasionally are moulded into flutes and so may be
364 contemporary with the end of FS3 (Fig. 4F2). As the eskers align with ice flow directions, we
365 favour esker formation by a time-transgressive build-up of sediment beneath a more slowly
366 retreating ISIS margin as opposed to instantaneous formation due to large meltwater floods,
367 which would see more frequent eskers in a larger range of directions (Hewitt, 2011).
368 Glacifluvial bedforms and associated sediments are sparsely distributed in Zone 2, limited to
369 these confined englacial/subglacial tunnels systems and isolated large depositional forms.
370 These forms include subaqueous fans formed against topographic highs that provided pinning
371 points for probably short-lived grounding-line stabilisation (Fig. 7). The restricted nature of
372 outwash deposits prevented potentially the burial of the glacial landscape of Zone 2. This
373 phase of warm-based ice streaming requires an ice-free western ISB, and is most likely
374 associated with the transition from geochronological Stage 3 to 4, between 21.4 ± 1.0 ka and
375 19.8 ± 0.8 ka BP during which the western and deeper (100–140 m bmsl) ISB had
376 deglaciated (Ballantyne and Ó Cofaigh, 2017; Chiverrell et al., 2018; McCabe, 2008).

377



378

379 Figure 7. A fan of proglacial sediments deposited down-ice from a bedrock outcrop.

380 The subglacial bedforms buried by the proglacial sediments were constructed by erosion into
381 bedrock and deposition of till.

382

383 **3.6 Ice margin retreat towards east and northeast**

384 Small ice-flow transverse ridges in a lobate planform overprint FS1–3 in the north of Zone 2
385 (Fig. 4G; 5G). Typically 5 m in height, 100–150 m in width and about 1 km long, these
386 regularly-spaced ridges are often broken up, but can be interpreted as ice marginal or
387 recessional moraines formed by small-scale oscillations of a retreating lobate ice margin. The
388 recessional moraines were the last grounded bedforms created in the area, with few flutes
389 discernible and probably reworked by moraine formation during retreat characterised by
390 backstepping and minor re-advances of the ice margin. Zones 1 and 2 are densely overprinted
391 by numerous well-preserved iceberg pits and elongated scour marks (Fig. 4I; Van
392 Landeghem et al., 2009), suggesting the generation of large numbers of icebergs and the
393 possible collapse of the ice stream in a subaqueous environment (Van Landeghem et al.,
394 2009). The eastern extent of the iceberg scour field coincides with a break in the background
395 topographic slope of the region at 40–50 m water depths, in turn matching the burial limits of
396 the glaciated terrain (Fig. 1B; 5I). A series of long moraines in Zone 4 (Fig. 1B; 4H;5H) are
397 interpreted as ice-front moraines formed parallel to the retreating ice margins. This last phase
398 of ice retreat is attributed here to geochronological Stages 4–5, and retreat of the ice margin
399 across the shallower (50–20 m bmsl) eastern ISB moving north across the Isle of Man
400 between 20.7 ± 0.7 and 19.3 ± 0.8 ka BP (Chiverrell et al., 2018).

401

402 **4. DISCUSSION**

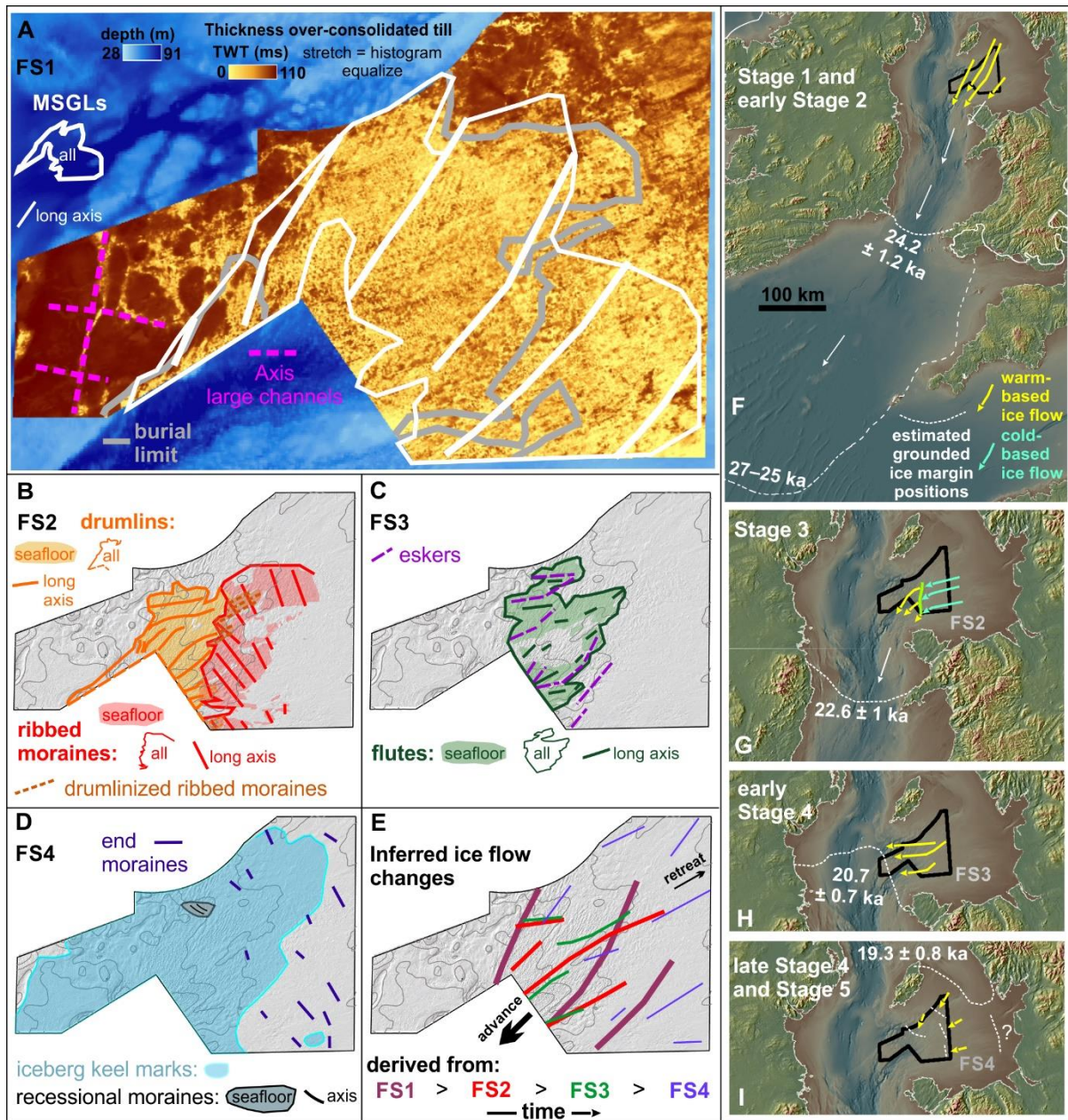
403 **4.1 Changing ice flow dynamics with evolution of the Irish Sea Ice Stream**

404 The evolution of the ISIS from 27 to 18 ka BP is described here in five chronological stages
405 (Section 1.2, and all the references herein). The ice-flow sets (FS) interpreted from glacial
406 bedform assemblages (Fig. 5J) are organised chronologically in Fig. 8E–I, contextualised

407 with these five stages of the advance and retreat. Ice flow is evidenced in Stage 1 (27–25 ka
408 BP) by large-scale MSGL (FS1 – Fig. 8A), providing the first definitive subglacial bedform
409 evidence for ice streaming within, and axis-parallel to, the ISB, and thus attributed to ice
410 margins located south of the Llŷn Peninsula – Wicklow constriction (Fig. 8F). Channelised
411 meltwater floods created large and deep tunnel valleys in Zone 1, at a time when meltwater
412 production under the ISIS potentially increased as ice flow was faster. The dataset presented
413 here shows two components to MSGL formation: subglacial erosion and till deformation.
414 During ISIS advance, bedrock erosion resulted in grooves and low-amplitude MSGLs,
415 leaving bedrock exposed on the ice–bed interface. A second and less erosive component to
416 MSGL formation left deformable till redistributed and deposited as crests of the MSGLs.
417 These two components must have occurred within the same flow phase as **the MSGL grooves**
418 **align perfectly with the crests**. The FS1 flow alignment and long MSGLs favour formation by
419 discharge of an ice stream thick enough to generate this erosion (cf. Motyka et al., 2006) and
420 to reach the Celtic Sea (e.g. Praeg et al., 2015; Lockhart et al., 2018 – Fig. 8F), at net advance
421 rates of $\sim 350 \text{ m a}^{-1}$ (Smedley et al., 2017a). MSGL formation probably continued during the
422 early phases of margin retreat (Stage 2), but then a significant change occurs. Analyses of
423 FS2 reveals a 20° and 60° change in ice flow direction, and formation of ribbed moraines
424 implies a slow-down in ice flow as they form in the ice stream onset zone where the bed is
425 frozen (e.g. Kleman and Hättestrand, 1999). At the end of Stage 3, ice margins retreated and
426 stabilised north of the Wicklow-Llŷn limit during early Stage 4, developing westerly ice flow
427 trajectories and oscillatory dynamics of the ice margin (Smedley et al., 2017a; Thomas and
428 Chiverrell, 2007), conditions that are consistent with observations from FS2 (Fig. 8b; 8G).
429 The drumlinisation has an erosional component carving into the bedrock surface (Fig. 4C; 7)
430 and delineates the onset of warm-based ice streaming in FS2. As Zone 2 is progressively
431 drumlinised (Fig. 5), faster ice was flowing (c.f. King et al., 2016; Smith and Murray, 2009)

432 from the shallow Zone 4 (Fig. 1B) towards accommodation space growing in the western ISB
433 (end of Stage 3). Drumlinisation was encouraged by the preceding ice stagnation during
434 ribbed moraine formation and the associated ice thickening providing sufficient frictional
435 heat to potentially melt basal ice and for the renewed ice streaming to deform the stiffer basal
436 diamictos. The timing of Stages 3 and 4 (22.6 ± 1 to 20.7 ± 0.7 ka BP) overlaps with cool
437 conditions in the North Atlantic (Rasmussen et al., 2014) and thermodynamic glacial
438 processes are thus favoured as the main driver for this flow-reactivation. This is an important
439 consideration in understanding present-day ice stream behaviour, as ice flow shut down and
440 abrupt changes in ice flow directions are observed and predicted to occur more frequently for
441 Antarctic ice streams (c.f. Conway et al., 2002). Fluting reflects a later realignment and last
442 phase of faster ice flow (FS3) at the start of Stage 4, which is attributed to ice surging into
443 deep waters to the west (Fig. 8C; 8H). The end of the fluting phase is associated with a
444 lubricated subglacial environment and extensive drainage patterns, with extensive iceberg
445 calving. The collapse of the ice stream was imminent with ice margin retreat patterns
446 seemingly topographically conditioned as small recessional moraines and large end-moraines
447 formed in a direction consistent with ice pulling back towards the Isle of Man and NW
448 England (Fig. 8D; 8I).

449 Sectors of the MSGL and ribbed moraine terrain were not drumlinised and we attribute this to
450 temporary lift-off of the ice bed in those areas driven by ice thinning due to intense iceberg
451 calving rather than sea level rise, which was probably limited over the estimated time of
452 grounding line fluctuations. Where the ice margin grounded again at the top of the break in
453 regional slope, it stagnated, with restricted calving and prolonged subglacial meltwater
454 drainage providing sediments to bury the eastern edge of the glacial terrain. Burial may have
455 continued during Stage 5, when Scottish ice re-advanced towards the northern edge of the
456 study area (Fig. 8D; 8I).



458

459 Figure 8. Summary geomorphology with Flow Sets (FS1–3) represented schematically. Panel
 460 (A) shows FS1 on over-consolidated glacial sediment thickness data in Two-Way-Travel
 461 Time (TWT) and with a stretched classification system using histogram equalisation to
 462 enhance contrast. Panels (B–E) display Flow Sets on contoured present-day seabed
 463 topography (see Fig. 1B). Panels F–I contextualises the temporal and spatial evolution of the
 464 palaeo-glacial landscape in the studied area (outlined in black) with the published

465 geochronology for the retreat of the former ISIS (see Section 1.2) to visualise the changes in
466 ice flow dynamics.

467

468 **4.2 Geological factors regulating ice sheet drainage?**

469 Our qualitative observations of changing bed conditions provide an insight into the link
470 between ice streaming and subglacial geological factors. Regional-scale erosion occurred into
471 the original till plateau and into the bedrock during formation of meltwater flow channels in
472 Zone 1 and the >30 km long MSGLs in Zone 2. In Zone 2, the deformable sediments were
473 largely removed where MSGLs were formed. This is evidenced through the integrated
474 interpretation of 16500 km of individual sub-bottom geophysical profiles (Fig. 4; 6; 8), where
475 the interpretation of the base of the over-consolidated glacial sediments (as gridded from
476 the seismic horizons) show clearly that the swathe of MSGLs is flanked to the west, north
477 and east by the remaining plateaus of over-consolidated till (Fig. 6; 8), where the deviated ice
478 flow path around the Isle of Man was likely most erosive in the immediate pathway of the
479 deviation. This pervasive erosional character in Stages 1 and 2 of ISIS advance and the initial
480 retreat agrees with observations beneath contemporary (Jezek et al., 2011) and palaeo-ice
481 streams with limited deformable sediment at the ice–bed (e.g. Bradwell, 2013; Krabbendam
482 et al., 2016; Smith, 1948). We suggest that the erosional processes involved during fast ice
483 streaming in the ISB induced a change in the geological factors steering the ice streaming, as
484 after the near complete removal of a deformable substrate from Zone 2, the bedrock became
485 exposed under the ice. These changes in ice–bed conditions would have adjusted ISIS
486 dynamics internally, as the style of basal sliding and subglacial drainage changes when the
487 bedrock underneath the eroded till is reached. Increased basal drag can slow down ice flows
488 and trigger basal freezing (c.f. Jacobson and Raymond, 1998). This may have happened to the
489 ISIS after formation of the MSGLs, because the ice bed must have frozen for ribbed moraines

490 to form. Passage of the ice margins northwards of the constriction between Wicklow and the
491 Llŷn Peninsula may also have contributed towards a slow-down in ice stream velocity. When
492 the downstream end of the retreating ISIS reached this area of exposed bedrock, the ice flow
493 changed direction with ribbed moraines and drumlins (FS2). The change from fast flow over
494 warm-based water-saturated soft diamict, to a temporarily compressional, re-aligned and
495 slower flow over cold-based and stiffer basal diamict is a significant change in ice stream
496 dynamics. These observations from the palaeo-ISIS agree with a recent sensitivity analyses in
497 ice stream models, finding changes in basal friction particularly influential for ice stream
498 dynamics when these changes are felt near the grounding zone (Alley et al., 2019). In our
499 case study, where the retreating palaeo-ISIS experienced topographical confinement and
500 where the western ISB started to become ice free, we propose that the changes in basal
501 friction will have been an additional contributing factor in ice stream shut-down, ice flow re-
502 alignment and ultimate demise.

503

504 **5. CONCLUSION**

505 The evolution of a well-preserved glacial landscape in the central part of a large palaeo-ice
506 stream details changes in ice flow dynamics during its advance and retreat that parallel
507 changes in ice thickness, ice bed conditions and proglacial open water accommodation space.
508 This reconstruction, linked to the robust geochronology of ice margin retreat, reveals that the
509 erosive ice stream processes exposed the bedrock underneath the ice during ice advance
510 and/or the early phases of deglaciation as MSGs were formed via an erosive and subsequent
511 depositional component within one ice-flow phase. We propose that the changes in basal
512 friction due to bedrock exposure to the ice may have contributed to defining the nature of
513 dynamics during deglaciation through slower ice flow velocities and basal freezing. During
514 later phases of deglaciation, topographic variations in the subglacial bed near the grounding

515 line increasingly conditioned ice flow as re-activation and re-alignment of ice streaming led
516 to an ultimate demise. This new analysis highlights that ice streaming can be determined by
517 how ice flow impacts local geology both prior to and during deglaciation, by altering the
518 availability of deformable bed and bed roughness underneath the ice. The dynamics of a
519 rapidly retreating palaeo-ice streams can thus be steered by the processes prior to the final
520 retreat phase, identifying a need for detailed parametrisation of ice–bed conditions throughout
521 all flow phases when forecasting episodes of changing retreat rate, shutdown and reactivation
522 of present-day ice streams, still the least understood components of ice sheet dynamics.

523

524 **ACKNOWLEDGMENTS**

525 The Crown Estate, a manager of the UK seabed, has published this offshore data on its online
526 Marine Data Exchange. This data has been gathered from surveys and technical studies from
527 the former Celtic Array offshore wind project off the coast of Anglesey in Wales, UK. Van
528 Landeghem acknowledges the financial support provided by the Welsh Government and
529 Higher Education Funding Council for Wales through the Sêr Cymru National Research
530 Network for Low Carbon, Energy and Environment.

531 The discussions with the reviewers have been a valuable contribution to this work, for which
532 the authors are grateful.

533

534 **REFERENCES**

- 535 Alley, R.B., Li, W., Parizek, B.R., Zhang, F., 2019. Evaluation of ice-stream model
536 sensitivities for parameter estimation. *Earth and Planetary Science Letters* 516, 49–55
- 537 Ballantyne, C.K., Ó Cofaigh, C., 2017. The last Irish Ice Sheet: extent and chronology,
538 *Advances in Irish Quaternary Studies*. Springer, pp. 101–149.

539 Bamber, J.L., Vaughan, D.G., Joughin, I., 2000. Widespread complex flow in the interior of
540 the Antarctic Ice Sheet. *Science* 287(5456), 1248–1250.

541 Bluemle, J.P., Lord, M.L. and Hunke, N.T., 1993. Exceptionally long, narrow drumlins
542 formed in subglacial cavities, North Dakota. *Boreas* 22(1), 15–24.

543 Bradley, S.L., Milne, G.A., Shennan, I. and Edwards, R., 2011. An improved glacial isostatic
544 adjustment model for the British Isles. *Journal of Quaternary Science* 26(5), 541–552.

545 Bradwell, T., 2013. Identifying palaeo-ice-stream tributaries on hard beds: Mapping glacial
546 bedforms and erosion zones in NW Scotland. *Geomorphology* 201, 397–414.

547 Bradwell, T., Small, D., Fabel, D., Smedley, R.K., Clark, C.D., Saher M.H., Callard, S.L.,
548 Chiverrell, R.C., Dove, D., Moreton, S.G., Roberts, D.H., Duller, G.A.T. and Ó
549 Cofaigh, C., 2019. Ice-stream demise dynamically conditioned by trough shape and
550 bed strength. *Science Advances* 5 (4).

551 Chiverrell, R.C., Smedley, R.K., Small, D., Ballantyne, C.K., Burke, M.J., Callard, S.L.,
552 Clark, C.D., Duller, G.A.T., Evans, D.J.A., Fabel, D., Van Landeghem, K.,
553 Livingstone, S., Ó Cofaigh, C., Thomas, G.S.P., Roberts, D.H., Saher, M., Scourse,
554 J.D. and Wilson, P., 2018. Ice margin oscillations during deglaciation of the northern
555 Irish Sea Basin. *Journal of Quaternary Science* 33(7), 739–762.

556 Chiverrell, R.C., Thrasher, I.M., Thomas, G.S.P., Lang, A., Scourse, J.D., Van Landeghem,
557 K.J.J., McCarroll, D., Clark, C.D., Ó'Cofaigh, C., Evans, D.J.A. and Ballantyne, C.K.,
558 2013. Bayesian modelling the retreat of the Irish Sea Ice Stream. *Journal of*
559 *Quaternary Science* 28(2), 200–209.

560 Conway, H., Catania, G., Raymond, C.F., Gades, A.M., Scambos, T.A. and Engelhardt, H.,
561 2002. Switch of flow direction in an Antarctic ice stream. *Nature* 419(6906), 465–
562 467.

563 Cuffey, K.M., Conway, H., Gades, A., Hallet, B., Raymond, C.F. and Whitlow, S., 2000.
564 Deformation properties of subfreezing glacier ice: Role of crystal size, chemical
565 impurities, and rock particles inferred from in situ measurements. *Journal of*
566 *Geophysical Research-Solid Earth* 105(B12), 27895–27915.

567 Evans, D.J.A. and Twigg, D.R., 2002. The active temperate glacial landsystem: A model
568 based on Breiðamerkurjökull and Fjallsjökull, Iceland. *Quaternary Science Reviews*
569 21(20–22), 2143–2177.

570 Hewitt, I.J., 2011. Modelling distributed and channelized subglacial drainage: The spacing of
571 channels. *Journal of Glaciology* 57(202), 302–314.

572 Hindmarsh, R.C.A., 2018. *Ice Sheet and Glacier Modelling, Past Glacial Environments*, pp.
573 605–661.

574 Hogan, K.A., Dowdeswell, J.A., Noormets, R., Evans, J. and Ó'Cofaigh, C., 2010. Evidence
575 for full-glacial flow and retreat of the Late Weichselian Ice Sheet from the waters
576 around Kong Karls Land, eastern Svalbard. *Quaternary Science Reviews* 29(25–26),
577 3563–3582.

578 Jacobson, H.P. and Raymond, C.F., 1998. Thermal effects on the location of ice stream
579 margins. *Journal of Geophysical Research: Solid Earth* 103(6), 12111–12122.

580 Jamieson, S.S.R., Vieli, A., Livingstone, S.J., Cofaigh, C.Ó., Stokes, C., Hillenbrand, C.D.
581 and Dowdeswell, J.A., 2012. Ice-stream stability on a reverse bed slope. *Nature*
582 *Geoscience* 5(11), 799–802.

583 Jamieson, S.S.R., Stokes, C.R., Livingstone, S.J., Vieli, A., Ó Cofaigh, C., Hillenbrand, C-D
584 and Spagnolo, M., 2016. Subglacial processes on an Antarctic ice stream bed. 2: Can
585 modelled ice dynamics explain the morphology of mega-scale glacial lineations?
586 *Journal of Glaciology* 62(232), 285–298

587 Jezek, K., Wu, X., Gogineni, P., Rodríguez, E., Freeman, A., Rodriguez-Morales, F. and
588 Clark, C.D., 2011. Radar images of the bed of the Greenland Ice Sheet. *Geophysical*
589 *Research Letters* 38(1), <https://doi.org/10.1029/2010GL045519>.

590 King, E.C., Hindmarsh, R.C.A. and Stokes, C.R., 2009. Formation of mega-scale glacial
591 lineations observed beneath a West Antarctic ice stream. *Nature Geoscience* 2(8),
592 585–588.

593 King, E.C., Pritchard, H.D. and Smith, A.M., 2016. Subglacial landforms beneath Rutford Ice
594 Stream, Antarctica: detailed bed topography from ice-penetrating radar. *Earth System*
595 *Science Data* 8(1), 151–158.

596 Kleman, J. and Applegate, P.J., 2014. Durations and propagation patterns of ice sheet
597 instability events. *Quaternary Science Reviews* 92, 32–39.

598 Kleman, J. and Glasser, N.F., 2007. The subglacial thermal organisation (STO) of ice sheets.
599 *Quaternary Science Reviews* 26(5–6), 585–597.

600 Kleman, J. and Hättestrand, C., 1999. Frozen-bed Fennoscandian and Laurentide ice sheets
601 during the Last Glacial Maximum. *Nature* 402(6757), 63–66.

602 Kleman, J., Hättestrand, C., Stroeven, A.P., Jansson, K.N., De Angelis, H. and Borgström, I.,
603 2006. Reconstruction of Palaeo-Ice Sheets-Inversion of their Glacial
604 Geomorphological Record. In: P.G. Knight (Editor), *Glacier science and*
605 *environmental change*. Blackwell Publishing, Malden, USA, pp. 192–198.

606 Krabbendam, M., Eyles, N., Putkinen, N., Bradwell, T. and Arbelaez-Moreno, L., 2016.
607 Streamlined hard beds formed by palaeo-ice streams: A review. *Sedimentary Geology*
608 338, 24–50.

609 Kurjanski, B., Rea, B.R., Spagnolo, M., Winsborrow, M., Cornwell, D.G., Andreassen, K.,
610 Howell, J., 2019. Morphological evidence for marine ice stream shutdown, central
611 Barents Sea. *Marine Geology* 414, 64–76

612 Lakeman, T.R., Pienkowski, A.J., Nixon, F.C., Furze, M.F.A., Blasco, S., Andrews, J.T. and
613 King, E.L., 2018. Collapse of a marine-based ice stream during the early Younger
614 Dryas chronozone, western Canadian Arctic. *Geology* 46(3), 211–214.

615 Landvik, J.Y., Alexanderson, H., Henriksen, M. and Ingolfsson, O., 2014. Landscape
616 imprints of changing glacial regimes during ice-sheet build-up and decay: a
617 conceptual model from Svalbard. *Quaternary Science Reviews* 92, 258–268.

618 Lee, J.R., Wakefield, O.J.W., Phillips, E. and Hughes, L., 2015. Sedimentary and structural
619 evolution of a relict subglacial to subaerial drainage system and its hydrogeological
620 implications: An example from Anglesey, north Wales, UK. *Quaternary Science*
621 *Reviews* 109, 88–110.

622 Lockhart, E.A., Scourse, J.D., Praeg, D., Van Landeghem, K.J.J., Mellett, C., Saher, M.,
623 Callard, L., Chiverrell, R., Benetti, S., Ó Cofaigh, C. and Clark, C.D. (2018). A
624 stratigraphic investigation of the Celtic Sea megaridges based on seismic and core
625 data from the Irish-UK sectors. *Quaternary Science Reviews*, 198, 156-170.

626 McCabe, A.M., 2008. *Glacial geology and geomorphology: the landscapes of Ireland*.
627 Dunedin Academic Press, Edinburgh, 274 pp.

628 Motyka, R.J., Truffer, M., Kuriger, E.M., Bucki, K., 2006. Rapid erosion of soft sediments by
629 tidewater glacier advance: Taku Glacier, Alaska, USA, *Geophys. Res. Lett.* 33,
630 L24504, doi:10.1029/2006GL028467.

631 Paterson, W.S.B., 1994. *The physics of glaciers*. Pergamon, Oxford.

632 Phillips, E., Everest, J. and Diaz-Doce, D., 2010. Bedrock controls on subglacial landform
633 distribution and geomorphological processes: Evidence from the Late Devensian Irish
634 Sea Ice Stream. *Sedimentary Geology* 232(3–4), 98–118.

635 Praeg, D., McCarron, S., Dove, D., Ó Cofaigh, C., Scott, G., Monteys, X., Facchin, L.,
636 Romeo, R. and Coxon, P., 2015. Ice sheet extension to the Celtic Sea shelf edge at the
637 Last Glacial Maximum. *Quaternary Science Reviews* 111, 107–112.

638 Rasmussen, S.O., Bigler, M., Blockley, S.P., Blunier, T., Buchardt, S.L., Clausen, H.B.,
639 Cvijanovic, I., Dahl-Jensen, D., Johnsen, S.J., Fischer, H., Gkinis, V., Guillevic, M.,
640 Hoek, W.Z., Lowe, J.J., Pedro, J.B., Popp, T., Seierstad, I.K., Steffensen, J.P.,
641 Svensson, A.M., Vallelonga, P., Vinther, B.M., Walker, M.J.C., Wheatley, J.J. and
642 Winstrup, M., 2014. A stratigraphic framework for abrupt climatic changes during the
643 Last Glacial period based on three synchronized Greenland ice-core records: Refining
644 and extending the INTIMATE event stratigraphy. *Quaternary Science Reviews* 106,
645 14–28.

646 Rignot, E., Mouginot, J., Morlighem, M., Seroussi, H. and Scheuchl, B., 2014. Widespread,
647 rapid grounding line retreat of Pine Island, Thwaites, Smith, and Kohler glaciers,
648 West Antarctica, from 1992 to 2011. *Geophysical Research Letters* 41(10), 3502–
649 3509.

650 Schoof, C. and Hewitt, I.J., 2016. A model for polythermal ice incorporating gravity-driven
651 moisture transport. *Journal of Fluid Mechanics* 797, 504–535.

652 Scourse, J., Saher, M., Van Landeghem, K., Lockhart, E.A., Purcell, C., Callard, L., Roseby,
653 Z., Allinson, B., Pienkowski, A.J., O Cofaigh, C., Praeg, D., Chiverrell, R.C.,
654 Moreton, S.G., Fabel, D. and Clark, C.D., 2019. Advance and retreat of the marine-

655 terminating Irish Sea Ice Stream into the Celtic Sea during the last glacial: timing and
656 maximum. *Marine Geology* 412, 53–68.

657 Small, D., Smedley, R.K., Chiverrell, R.C., Scourse, J.D., Cofaigh, C., Duller, G.A.T.,
658 McCarron, S., Burke, M.J., Evans, D.J., Fabel, D., Gheorghiu, D.M., Thomas, G.S.P.,
659 Xu, S. and Clark, C.D., 2018. Trough geometry was a greater influence than climate-
660 ocean forcing in regulating retreat of the marine-based Irish-Sea Ice Stream. *Bulletin*
661 *of the Geological Society of America* 130(11–12), 1981–1999.

662 Smedley, R.K., Chiverrell, R.C., Ballantyne, C.K., Burke, M.J., Clark, C.D., Duller, G.A.T.,
663 Fabel, D., McCarroll, D., Scourse, J.D., Small, D. and Thomas, G.S.P., 2017a.
664 Internal dynamics condition centennial-scale oscillations in marinebased ice-stream
665 retreat. *Geology* 45(9), 787–790.

666 Smedley, R.K., Scourse, J.D., Small, D., Hiemstra, J.F., Duller, G.A.T., Bateman, M.D.,
667 Burke, M.J., Chiverrell, R.C., Clark, C.D., Davies, S.M., Fabel, D., Gheorghiu, D.M.,
668 McCarroll, D., Medialdea, A. and Xu, S., 2017b. New age constraints for the limit of
669 the British–Irish Ice Sheet on the Isles of Scilly. *Journal of Quaternary Science* 32(1),
670 48–62.

671 Smith, A.M., Bentley, C.R., Bingham, R.G. and Jordan, T.A., 2012. Rapid subglacial erosion
672 beneath Pine Island Glacier, West Antarctica. *Geophysical Research Letters* 39(12).

673 Smith, A.M. and Murray, T., 2009. Bedform topography and basal conditions beneath a fast-
674 flowing West Antarctic ice stream. *Quaternary Science Reviews* 28(7–8), 584–596.

675 Smith, A.M., Murray, T., Nicholls, K.W., Makinson, K., Adalgeirsdóttir, G., Behar, A.E. and
676 Vaughan, D.G., 2007. Rapid erosion, drumlin formation, and changing hydrology
677 beneath an Antarctic ice stream. *Geology* 35(2), 127–130.

678 Smith, H.T.U., 1948. Giant glacial grooves in northwest Canada. *American Journal of*
679 *Science* 246(8), 503–514.

680 Spagnolo, M., Clark, C.D., Ely, J.C., Stokes, C.R., Anderson, J.B., Andreassen, K.,
681 Graham, A.G.C., King, E.C., 2014. Size, shape and spatial arrangement of mega-scale
682 glacial lineations. *Earth Surface Processes and Landforms* 39, 1432–1448.

683 Stokes, C.R., 2018. Geomorphology under ice streams: Moving from form to process. *Earth*
684 *Surface Processes and Landforms* 43(1), 85–123.

685 Stokes, C.R. and Clark, C.D., 2002. Are long subglacial bedforms indicative of fast ice flow?
686 *Boreas* 31, 239–249.

687 Stroeven, A.P., Hättestrand, C., Kleman, J., Heyman, J., Fabel, D., Fredin, O., Goodfellow,
688 B.W., Harbor, J.M., Jansen, J.D., Olsen, L., Caffee, M.W., Fink, D., Lundqvist, J.,
689 Rosqvist, G.C., Strömberg, B. and Jansson, K.N., 2016. Deglaciation of
690 Fennoscandia. *Quaternary Science Reviews* 147, 91–121.

691 Thomas, G.S.P. and Chiverrell, R.C., 2007. Structural and depositional evidence for repeated
692 ice-marginal oscillation along the eastern margin of the Late Devensian Irish Sea Ice
693 Stream. *Quaternary Science Reviews* 26(19–21), 2375–2405.

694 Tóth, Z., McCarron, S., Wheeler, A.J., Wenau, S., Davis, S., Lim, A. and Spiess, V., 2020.
695 Geomorphological and seismostratigraphic evidence for multidirectional polyphase
696 glaciation of the northern Celtic Sea. *Journal of Quaternary Sciences* 35, 465–478.

697 Van Landeghem, K.J.J., Wheeler, A.J. and Mitchell, N.C., 2009. Seafloor evidence for
698 palaeo-ice streaming and calving of the grounded Irish Sea Ice Stream: Implications
699 for the interpretation of its final deglaciation phase. *Boreas* 38(1), 111–131.

700 Waller, R.I., Van Dijk, T.A.G.P. and Knudsen, Ó., 2008. Subglacial bedforms and conditions
701 associated with the 1991 surge of Skeiðarárjökull, Iceland. *Boreas* 37(2), 179–194.

702 Ward, S.L., Neill, S.P., Scourse, J.D., Bradley, S.L. and Uehara, K., 2016. Sensitivity of
703 palaeotidal models of the northwest European shelf seas to glacial isostatic adjustment
704 since the Last Glacial Maximum. *Quaternary Science Reviews* 151, 198–211.